

Antiferromagnetism in the magnetoelectric effect single crystal LiMnPO_4

Jiying Li^{1,2}, Wei Tian³, Ying Chen^{1,2}, Jerel L. Zarestky³, Jeffrey W. Lynn¹, and David Vaknin^{3*}

¹*NIST Center for Neutron Research, National Institute of Standards and Technology, Gaithersburg, MD 20899*

²*Department of Materials Science and Engineering,
University of Maryland, College Park, MD 20742*

³*Ames Laboratory and Department of Physics and Astronomy, Iowa State University, Ames, IA 50011*

(Dated: November 5, 2018)

Elastic and inelastic neutron scattering studies reveal details of the antiferromagnetic transition and intriguing spin-dynamics in the magneto-electric effect single crystal LiMnPO_4 . The elastic scattering studies confirm the system is antiferromagnetic (AFM) below $T_N=33.75$ K with local magnetic moments (Mn^{2+} ; $S = 5/2$) that are aligned along the crystallographic a -axis. The spin-wave dispersion curves propagating along the three principal axes, determined by inelastic scattering, are adequately modeled in the linear spin-wave framework assuming a spin-Hamiltonian that is parameterized by inter- and in-plane nearest- and next-nearest-neighbor interactions, and by easy-plane anisotropy. The temperature dependence of the spin dynamics makes this an excellent model many-body spin system to address the question of the relationship between spin-wave excitations and the order parameter.

PACS numbers: 75.25.+z, 75.30.Ds, 75.50.Ee

INTRODUCTION

The recent discoveries of colossal magnetoelectric effects (ME) in rare-earth-manganites (RMnO_3 [1, 2]) and manganese-oxides (R_2MnO_5 [3]) triggered a revival interest in the so-called insulating multiferroic materials that exhibit ferroelectricity in coexistence with ferromagnetism or antiferromagnetism (FM or AFM) [4, 5]. Systematic studies of the coupling between the electric and magnetic fields in crystals date back to the early 1960s with the discovery of the first ME compound Cr_2O_3 [6, 7]. Early on, the isostructural transition-metal lithium-orthophosphates LiMPO_4 ($M = \text{Mn, Fe, Co, Ni}$) were identified as ME systems [8, 9, 10] and have been the subjects of numerous studies [11, 12, 13]. Like other members of the lithium-orthophosphates, LiMnPO_4 is an antiferromagnetic insulator with $Pnma$ symmetry group [14, 15]. In this structure, each Mn^{2+} ion occupies the center of a slightly distorted MnO_6 octahedron that shares oxygen anions with a tetrahedral PO_4 forming a closely packed oxygen framework. The Mn^{2+} ions ($S = 5/2$) form buckled layers that are stacked along the [100] crystallographic axis, as shown in Fig. 1(a). The nearest neighbors (NN) in the b - c plane are coupled magnetically by a relatively strong exchange interaction J_1 through an Mn-O-Mn oxygen-bond, whereas the in-plane next-NN (NNN) are coupled via Mn-O-O-Mn (J_2) [16, 17] (see Fig. 1(b) for the definitions of the exchange couplings). The interlayer magnetic coupling is mediated through phosphates by higher order superexchange via Mn-O-P-O-Mn, which was found to be relatively large in similar frameworks [18].

Neutron diffraction of polycrystalline samples [19, 20, 21] and single crystal NMR [16] measurements showed that all LiMPO_4 share the same collinear (up-down) AFM ground state with spin orientation along a , b , b and c crystallographic directions for LiMnPO_4 , LiFePO_4 , LiCoPO_4 and LiNiPO_4 , respectively. However, recent single crystal neutron diffraction studies of LiCoPO_4 , LiFePO_4 , and LiNiPO_4 , [22, 23, 24, 25] show the moments in the ground state are slightly tilted away from principal crystallographic directions, indicating the magnetic symmetries for these systems are lower than those determined from polycrystalline measurements, giving rise to spontaneously induced weak ferromagnetism. Weak ferromagnetism (WFM) in magnetic susceptibility measurements has also been reported for LiNiPO_4 [26] and LiMnPO_4 [27] below T_N . Indeed, domain structures observed by second-harmonic-generation (SHG) experiments in LiCoPO_4 were interpreted as ferrotoroidic domains [28] facilitated by the lower magnetic symmetry obtained in neutron scattering experiments [22]. Based on the detailed spin configuration observed in LiNiPO_4 , Jensen and co-workers have been able to model the temperature dependence of the ME coefficients of this system [25].

Here, we report elastic and inelastic neutron scattering studies of a single crystal LiMnPO_4 , to determine the nature of the AFM transition and the spin dynamics in this system. Recent susceptibility measurements indicated WFM in this system [27] implying spin-canting that may be detected in neutron diffraction measurements. There is also some inconsistency in the literature with regard to the transition temperature; $T_N = 34.85$ [19, 20] and 42 K were reported [27] for polycrystalline samples. The spin dynamics of the LiFePO_4 , LiCoPO_4 and LiNiPO_4 were measured and modeled in the linear spin-wave framework only recently [23, 24, 29], to suc-

*electronic mail: vaknin@ameslab.gov

cessfully yield the exchange couplings and the single-ion anisotropy parameters in these systems. Determining and analyzing the spin dynamics of LiMnPO_4 is an important step towards developing a universal understanding of the magnetic properties of this isostructural group of compounds.

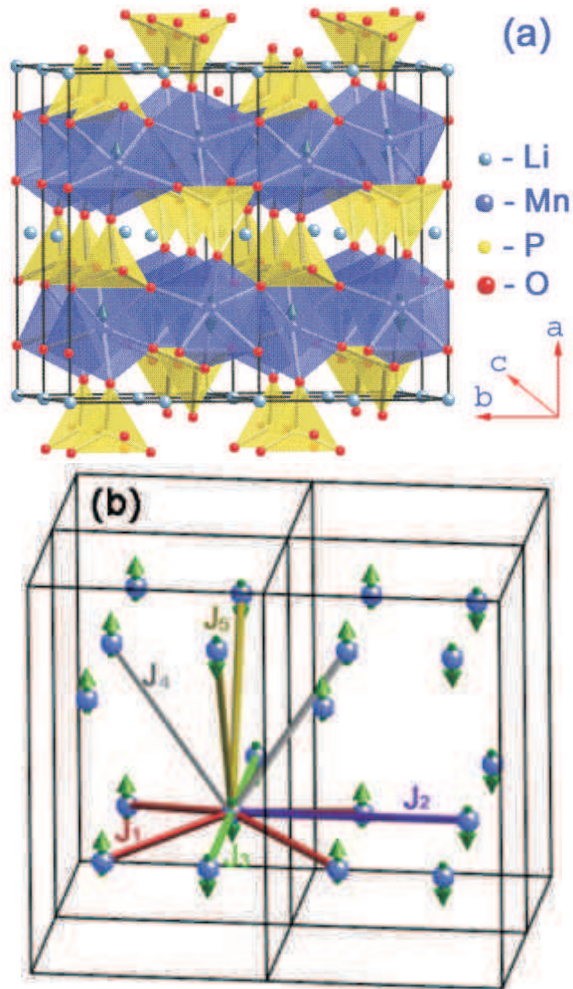


FIG. 1: (color online) (a) Atomic structure of LiMnPO_4 . The Mn^{2+} ions form buckled layers stacked perpendicular to the $[100]$ crystallographic direction. The ground state of LiMnPO_4 is collinear antiferromagnetic with average moments along the *a*-axis. (b) Spin arrangement of the two Mn^{2+} layers. The in-plane nearest and next-nearest neighbor interactions J_1 , J_2 , J_3 and inter-plane nearest and next-nearest neighbor interactions J_4 , J_5 are labeled.

EXPERIMENTAL DETAILS

A LiMnPO_4 single crystal (0.41 gram, pink in color) was grown by the standard flux growth technique (LiCl was used as the flux) from a stoichiometric mixture of high purity MnCl_2 (99.999% Aldrich) and Li_3PO_4

(99.999% Aldrich) [30]. Powder, for the XRD, was prepared by crushing typical isolated single crystals. The composition and structure were confirmed by carrying out Rietveld analysis of X-ray powder diffraction (XRD) data, using the GSAS software package [31]. No extra peaks from impurities were detected in the XRD pattern. The lattice parameters yielded from the refinement at room temperature ($a = 10.524 \text{ \AA}$, $b = 6.095 \text{ \AA}$, and $c = 4.75 \text{ \AA}$) are in good agreement with the values reported in the literatures [20, 32, 33].

Neutron scattering measurements were carried out on the BT7 and BT9 thermal triple axis spectrometer at the National Institute of Standards and Technology (NIST) Center for Neutron Research (NCNR). A monochromatic neutron beam of wavelength $\lambda = 2.36 \text{ \AA}$ (14.7 meV, $k_o = 2\pi/\lambda = 2.66 \text{ \AA}^{-1}$) was selected by a vertical focusing monochromator system, using the $(0\ 0\ 2)$ Bragg reflection of highly oriented pyrolytic graphite (HOPG) crystals. HOPG crystals were also used as analyzer for both the elastic and the inelastic studies. The high resolution inelastic scattering measurements were conducted on the cold neutron Spin Polarized Inelastic Neutron Spectrometer (SPINS) at the NCNR.

RESULTS AND DISCUSSION

Elastic neutron scattering

The LiMnPO_4 crystal was oriented with its *a*-*b* plane, (and subsequently rotated with its *b*-*c* plane) to coincide with the scattering-plane of the spectrometer. The elastic measurements, with the strongest magnetic reflection (010) peak, confirmed that the magnetic structure of LiMnPO_4 is AFM with spin orientation along the *a*-axis.

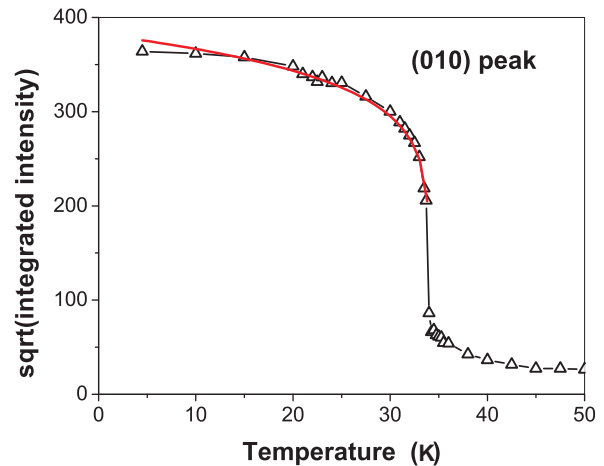


FIG. 2: (Color online) Temperature dependence of the square root of the integrated intensity of the (010) magnetic peak. The transition temperature obtained from the fit is $T_N = 33.85 \pm 0.1 \text{ K}$ and the critical exponent $\beta = 0.126 \pm 0.017$.

The temperature dependence of the magnetic (010) reflection was used to extract the behavior of the order parameter in the temperature range from 5 to 50 K. Figure 2 shows the square root of the integrated intensity, representing the staggered magnetization, (i.e., order parameter) as a function of temperature for the (010) peak. The order parameter was fit to a power law function near the transition temperature:

$$\sqrt{I} \propto M^\dagger = M_0^\dagger t^\beta \quad (1)$$

where M_0^\dagger is the sublattice magnetization at $T = 0$ K, $t = (1 - T/T_N)$ is the reduced temperature, and β is the critical exponent. The obtained transition temperatures from the fit is $T_N = 33.85 \pm 0.1$ K and the critical exponent for the temperature dependent magnetization β is 0.126 ± 0.017 by using the main (010) magnetic peak. This is very close to the theoretical value of the critical exponent of the 2D Ising system $\beta = 0.125$ [34], consistent with the layered nature of the magnetic system, as also demonstrated by the weak interlayer coupling obtained from the analysis of the spin-waves discussed below. The transition temperature is found to be very close to the value, 34.85 ± 0.1 K measured by Mays [16] using nuclear magnetic resonances performed on a single crystal of LiMnPO_4 , whereas susceptibility measurements of powder samples yield $T_N = 42$ K [27].

Unlike LiCoPO_4 and LiFePO_4 , strong critical scattering above the AFM transition is observed in LiMnPO_4 and persists to almost twice T_N (traced to temperatures as high as 70 K) before the spins become uncorrelated. These correlations were already evident in Figure 2. Figure 3 shows longitudinal and transversal scans at the (010) magnetic peak above the transition with energy transfer $\Delta E = 0$. The peaks are much broader than the spectrometer's resolution indicating some type of short range correlations. This is reminiscent of the behavior in LiNiPO_4 where this critical scattering [21] was later found to be associated with an incommensurate (IC) short- and long-range magnetic order above T_N [35]. Below ~ 33 K all peaks are practically resolution limited Gaussian shaped. Above T_N , the peaks were fit to a Lorentzian line shape $1/(q^2 + \kappa^2)$, where $q = h$ or k , and κ is inversely proportional to the coherence length $\xi = 2\pi/\kappa$, convoluted with an instrumental gaussian shaped resolution function. The calculated coherence lengths along the a - and b -axis, as a function of temperature are shown in Figure 3 (c). Below the transition temperature, the in-plane coherence lengths (along the b -axis) is significantly longer than that between the planes (along the a -axis), consistent with the quasi-2D nature of LiMnPO_4 . The correlation lengths were remeasured on BT9 using the integrated energy (two-axis mode) method and yielded similar results. Attempts to correlate the in-plane coherence length in the critical regime with the 2D-Ising model failed, but the Kosterlitz-Thouless (KT) 2D XY-model, $\xi(T) = Ae^{B/(T-T_c)^v}$, seems to fit our data

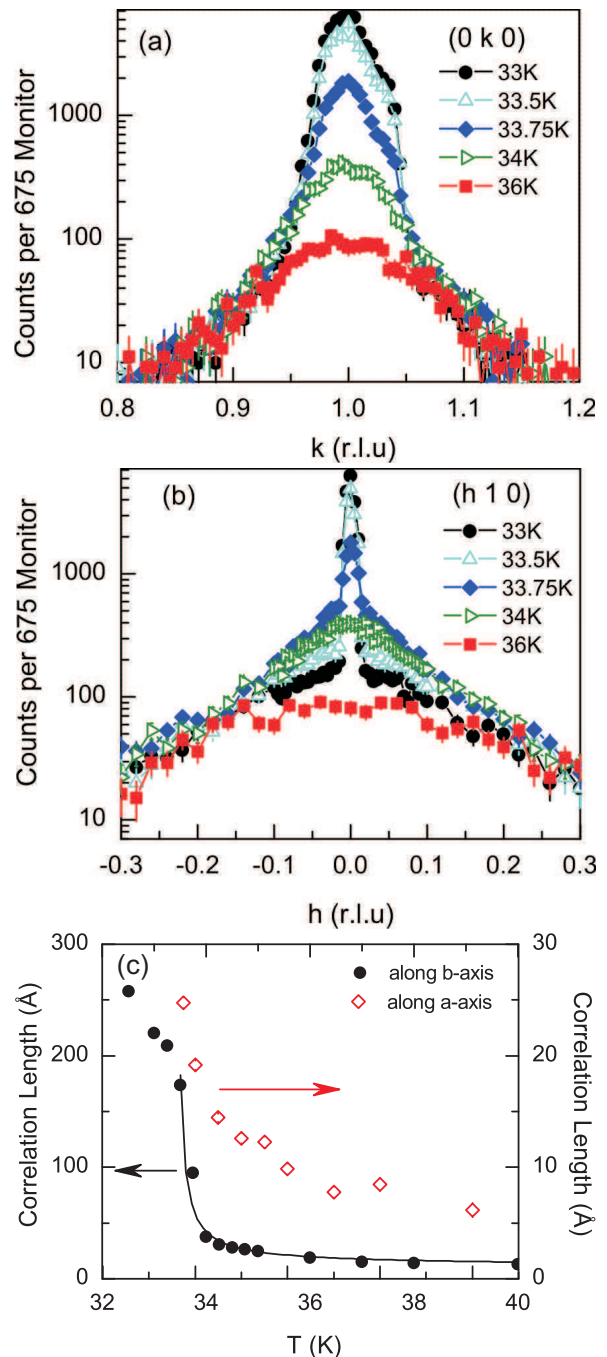


FIG. 3: (Color online) (a) Longitudinal and (b) transversal, (i.e., inter-plane) critical magnetic scattering scans at the (010) magnetic reflection above T_N . (c) Correlation lengths obtained after deconvoluting the spectrometer's resolution function (in-plane and inter-plane as indicated) versus temperature. Solid line is calculated assuming Kosterlitz-Thouless theory. The error bars in this paper are statistical in origin and represent one standard deviation. (r.l.u. stands for reciprocal lattice unit)

well [36] (solid line, Fig. 3) with $T_c = 33.6 \pm 0.008$ and $v = 0.51 \pm 0.1$. This strong critical scattering above the transition with KT characteristics may therefore indicate

spin-dimensionality crossover from the 2D Heisenberg to the 2D XY-model.

Inelastic and quasielastic neutron scattering

Spin waves along the three principal reciprocal lattice directions $(q, 1, 0)$, $(0, 1+q, 0)$ and $(0, 1, q)$ were measured in energy loss mode at $T = 5$ K. Examples of the excitations measured on BT7 at $q = 0.2$ are shown in Figure 4. A single excitation was observed at each q along the three directions on BT7 which has an energy resolution of ~ 1 meV. At $T \approx 50$ K, no similar peaks are observed confirming the magnetic origin of the excitations. The inelastic signals at various constant wave-vectors q were fit to Gaussian shaped functions (solid line in Fig. 4), and the set of energies at maximum intensity were used to construct the spin-wave dispersion curves shown in Fig. 6. It is shown that the spin-waves propagating in the plane along the (001) and (010) directions have higher energy than the spin-waves propagating along (100) at the same q values. Qualitatively, this behavior reflects the anisotropy in the strength of the exchange couplings in the system; as expected, the in-plane exchange couplings are much stronger than those between planes. Using the cold neutron triple axis SPINS spectrometer, an energy gap $E_G = 0.48$ meV was observed around the (010) zone center, which is much smaller than the 2 meV [29], 5.86 meV [23], and 4.7 meV [24] observed in LiNiPO₄, LiFePO₄ and LiCoPO₄, respectively. With the high energy resolution of SPINS, which is around 0.1 meV (using 3.7 meV final energy), two energy excitation peaks were identified at the zone center, as shown in Figure 5.

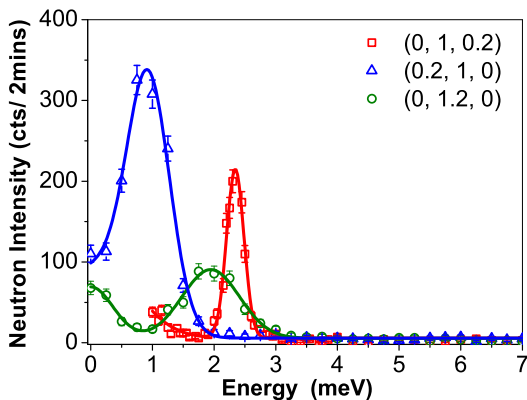


FIG. 4: (color online) Examples of constant-Q energy scans measured on BT7 at 5 K, at wave-vectors $q = 0.2$ along $(q, 1, 0)$, $(0, 1+q, 0)$ and $(0, 1, q)$ reciprocal directions. A single energy excitation is present in every direction with the typical energy resolution of BT7 around 1 meV.

To model the spin-wave dispersions, we use a spin

Hamiltonian based on the ground state spin structure of LiMnPO₄ as shown in Fig. 1, as follows

$$\mathcal{H} = \sum_{i,j} (J_{\{i,j\}} \mathbf{S}_i \cdot \mathbf{S}_j) + \sum_{i,\xi} D_{\xi} (S_i^{\xi})^2 \quad (2)$$

J_1 to J_5 are the spin coupling constants (see Fig. 1), and D_{ξ} are the single ion anisotropies. Since the excitation spectrum is insensitive to an overall shift of the ground state energy we can define $D_z \equiv 0$ for simplicity. The x, y , and z coordinates are defined along the c -, b - and a -axis, respectively, to align the spin direction in the ground state with the quantum z -axis in Eq. (2). The magnon dispersion curves derived from Eq. (2) by linear spin-wave theory is given in Refs [23, 29, 37]. In the model, the calculated spin waves have two non-degenerate branches (denoted by the \pm sign in Eq. 3) as a result of the different anisotropies along the x and y directions.

$$\hbar\omega = \sqrt{A^2 - (B \pm C)^2} \quad (3)$$

where,

$$A \equiv 4S(J_1 + J_5) - 2S[J_3(1 - \cos(\mathbf{q} \cdot \mathbf{r}_5)) + J_2(1 - \cos(\mathbf{q} \cdot \mathbf{r}_6)) + J_4(2 - \cos(\mathbf{q} \cdot \mathbf{r}_7) - \cos(\mathbf{q} \cdot \mathbf{r}_8))] + (S - 1/2)(D_x + D_y),$$

$$B \equiv (S - 1/2)(D_x - D_y),$$

$$C \equiv 2J_1S[\cos(\mathbf{q} \cdot \mathbf{r}_1) + \cos(\mathbf{q} \cdot \mathbf{r}_2)] + 2J_5S[\cos(\mathbf{q} \cdot \mathbf{r}_3) + \cos(\mathbf{q} \cdot \mathbf{r}_4)],$$

and \mathbf{r}_i denotes a vector to a NN and NNN,

$$\begin{aligned} \mathbf{r}_1 &= (c/2, b/2, 0) & \mathbf{r}_2 &= (-c/2, b/2, 0) \\ \mathbf{r}_3 &= (0, b/2, a/2) & \mathbf{r}_4 &= (0, -b/2, a/2) \\ \mathbf{r}_5 &= (0, b, 0) & \mathbf{r}_6 &= (c, 0, 0) \\ \mathbf{r}_7 &= (c/2, 0, a/2) & \mathbf{r}_8 &= (-c/2, 0, a/2). \end{aligned}$$

The spin-wave dispersion curves along the three directions in Fig. 6 were simultaneously fit to Eq. (3), using the “-” sign, yielding the following values: $J_1 = 0.48 \pm 0.05$ meV, $J_2 = 0.2 \pm 0.038$ meV, $J_3 = 0.076 \pm 0.004$ meV, $J_4 = 0.036 \pm 0.002$ meV, $J_5 = 0.062 \pm 0.003$ meV, $D_x = 0.0069 \pm 0.001$ meV and $D_y = 0.0089 \pm 0.001$ meV. In the equation, $S = 5/2$ for Mn²⁺. As expected, the in-plane NN exchange coupling J_1 , is the strongest, compared to the in-plane NNNs J_2 and J_3 . The sign of both J_2 and J_3 indicates the NNN interactions compete with the simple AFM ordering dictated by J_1 . For weakly coupled layers, it has been predicted theoretically that an incommensurate (IC) magnetic structure should be realized when $J_2/J_1 > 0.5$ [38]. Thus, unlike in LiNiPO₄

where the $J_2/J_1 \approx 0.6$ and an IC has been observed, the ratio for LiMnPO_4 (~ 0.4) seems to be too small to induce any IC phase transition [29]. The spin couplings between the inter-plane nearest-neighbors (J_4 and J_5) are relatively weak at about 12% of J_1 consistent with the quasi-2D behavior of this system. The values of the single ion $D_x = 0.0055$ and $D_y = 0.0071$, are much smaller than those of LiNiPO_4 [29], LiFePO_4 [23], and LiCoPO_4 [24] indicating that the ground state with magnetic moments along the a -axis is not very stable, and the moments are prone to a spin-flop transition in relatively weak magnetic fields [39, 40].

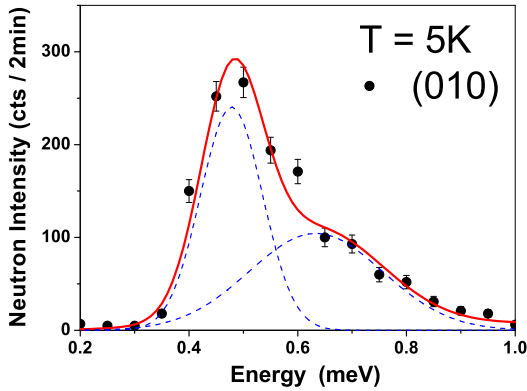


FIG. 5: (color online) The energy excitation at the zone center measured on SPINS cold neutron triple axis which has an energy resolution of ~ 0.1 meV. Two excitations are clearly identified at the zone center.

The second spin wave dispersion branches, given by “+” sign in Eq. (3), are calculated using the J s and D s obtained from the fits listed above. The two branches almost overlap one another for the dispersions along all the three principal reciprocal directions, and are only separate by ~ 0.1 meV at the zone center. The spin wave dispersion along $(q, 1, 0)$ direction, where the model predicts the largest separation between the two branches, was re-measured with the high energy resolution on SPINS. Figure 6 (b) shows an enlargement graph of Figure 6 (a), with fairly good agreement with the model calculations.

The energy gaps at the zone center for the two branches are

$$\Delta E = 2S\sqrt{4D_x(J_1 + J_5) + D_x D_y}, \quad (4)$$

for (B - C) in Eq. (3) and

$$\Delta E = 2S\sqrt{4D_y(J_1 + J_5) + D_x D_y}, \quad (5)$$

for (B + C). J_5 represents the inter-plane NN coupling. From the equations, we notice that the energy gap not only depends on the single-ion anisotropy terms, but also on the two nearest-neighbor antiparallel exchange interactions.

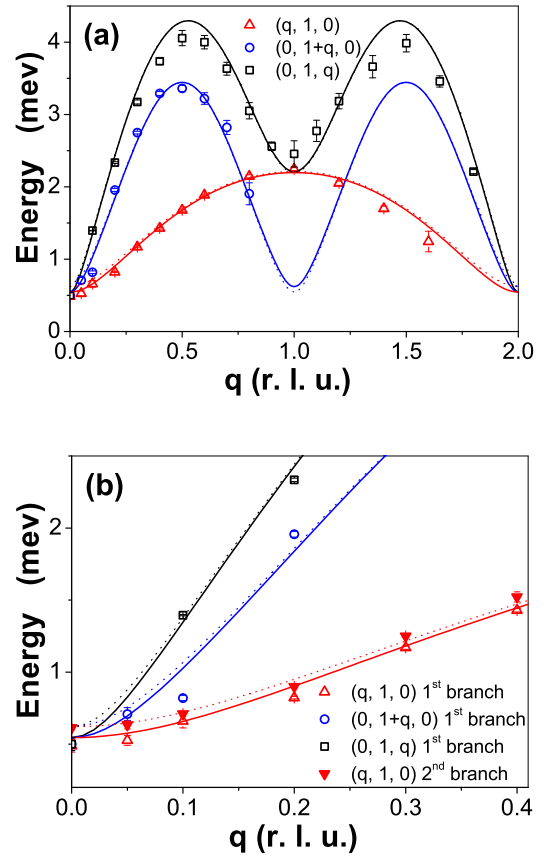


FIG. 6: (color online) (a) Spin-wave dispersion curves along the a^* , b^* , and c^* reciprocal space directions measured at 5 K. Solid lines are best-fit calculations obtained from linear spin-wave theory using Eq. (3). (b) Zoomed plot of (a) near the zone center. The predicted second spin wave dispersion branches are shown as dashed lines.

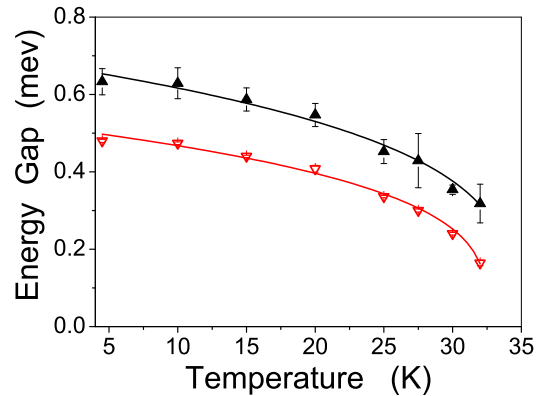


FIG. 7: (Color online) The energy gap as a function of temperature measured on the SPINS cold neutron triple axis.

The temperature dependent energy gap up to the tran-

sition temperature was measured at the cold neutron triple axis spectrometer SPINS, and the results are shown in Figure 7 (energy gaps at various temperatures were determined from gaussian fits to constant-Q energy scans such as the one shown in Fig. 5 at $T = 5$ K). The energy gap monotonically decreases with increasing temperature and approaches zero at the transition temperature. The temperature dependence of the gap to a first approximation is proportional to the staggered magnetization which is temperature dependent[42]. However, it may deviate in the critical regime due to the different temperature dependencies of the coupling constants and the single ion anisotropy. In antiferromagnets, the exchange constants J_s usually decrease much faster than the single ion anisotropy near the transition temperature [41, 42].

Quasi-elastic scattering (QENS) around (010) at different temperatures was measured on BT9 using the integrated energy (two-axis) mode, and the results are shown in Figure 8. At temperatures right below the transition, the (010) peak consists of a resolution limited Gaussian shaped magnetic Bragg peak superimposed on a broad Lorentzian shaped diffuse peak. Whereas the diffuse scattering becomes stronger with the increase of temperature (up to the transition), the elastic magnetic Bragg peak becomes weaker. The QENS intensity at each temperature was integrated over the the K range shown in Figure 8 (a) excluding the region from 0.98 to 1.02 (r.l.u) which is dominated by elastic scattering. Figure 8 (b) shows the QENS as a function of temperature, which exhibits a sharp peak at the transition ($T_N = 33.75$ K) with a tail that extends to about $1.5T_N$. This indicates that the short range correlations observed in the elastic scattering are primarily due to (dynamics) spin-fluctuations.

In summary, we determined the critical behavior near the AFM magnetic phase transition of LiMnPO_4 ($T_N = 33.85$ K). The strong critical scattering around the (010) magnetic peak and the in-plane, inter-plane coherence lengths indicate that the system is a quasi-2D system with very weak easy axis single ion anisotropy. Analysis of the spin-wave dispersions along the three principal axis directions show that the in-plane couplings are dominant compared to the inter-plane couplings. These in-plane competing interactions between in-plane NN and NNN-spins in LiMnPO_4 seem to be too weak to lead to more complicated, incommensurate magnetic structures. This is in contrast to the observation of incommensurate magnetic phases in LiNiPO_4 [35].

We thank Sung Chang for the support on the SPINS cold neutron triple axis. Ames Laboratory is supported by the U.S. Department of Energy, Basic Energy Sciences, Office of Science, under Contract No. DE-AC02-07CH11358. SPINS is supported in part by the US National Science Foundation through DMR-0454672.

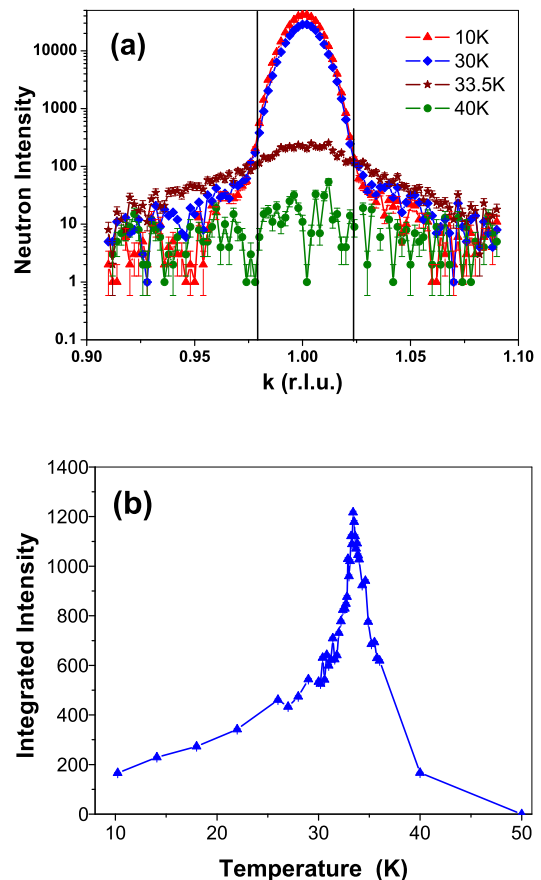


FIG. 8: (Color online)(a) Examples of the quasielastic scattering scans around (010) magnetic peak at temperatures below and above the transition temperature T_N , which were measured on BT9 using the integrated energy method. (b) The temperature dependent integrated intensity from the quasielastic scattering excluding $Q = 0.98$ to 1.02 as indicated by the box in (a).

-
- [1] T. Kimura, T. Goto, H. Shintani, K. Ishizaka, T. Arima, and Y. Tokura, *Nature* **426**, 55 (2003).
 - [2] T. Goto, T. Kimura, G. Lawes, A. P. Ramirez, and Y. Tokura, *Phys. Rev. Lett.* **92**, 257201 (2004).
 - [3] N. Hur, S. Park, P. A. Sharma, S. Guha, and S. W. Cheong, *Phys. Rev. Lett.* **93**, 107207-1 (2004).
 - [4] M. Fiebig, *J. Phys. D: Appl. Phys.*, **38**, R123 (2005).
 - [5] W. Eerenstein, N. D. Mathur, and J. F. Scott, *Nature* **442**, 759 (2006).
 - [6] D. N. Astrov, *J. Exp. Theoret. Phys. (U.S.S.R.)* **38**, 984 (1960).
 - [7] G. T. Rado and V. J. Folen, *Phys. Rev. Lett.* **7**, 310 (1961).
 - [8] M. Mercier, and J. Gareyte, *Sol. State Comm.* **5**, 139 (1967); **7**, 149 (1969).
 - [9] M. Mercier, and P. Bauer, *C. R. Acad. Sci. Paris* **267**, 465 (1968); and M. Mercier, Ph.D. thesis, Universit de

- Grenoble, 1969.
- [10] J. -P. Rivera, *Ferroelectrics* **161**, 147 (1994).
- [11] *Magnetoelectric interaction phenomena in crystals*, edited by A.J. Freeman and H. Schmid (Gordon and Breach Science Publishers, London/New York, 1975); references therein.
- [12] Proceedings of the Second International Conference on Magnetoelectric Interaction Phenomena in Crystals (MEIPIC-2), Ascona, 1993, Parts I and II, edited by H. Schmid, A. Janner, H. Grimmer, J.-P. Rivera, and Z.-G. Ye [*Ferroelectrics* **161**, 1 (1994); **162**, 1 (1994)], references therein.
- [13] *Magnetoelectric Interactions Phenomena in Crystals*, edited by M. Fiebig, V. V. Eremenko, and I. E. Chupis, NATO Science Series (Kluwer Academic Publishers, Dordrecht, 2004); references therein.
- [14] S. Geller and J. L. Easson, *Acta Crystallogr.*, **18**, 258 (1960).
- [15] H. D. Megaw, *Crystal Structures - A Working Approach*, Saunders, Philadelphia, 1973, P249.
- [16] J. M. Mays, *Phys. Rev.* **131**, 38 (1963).
- [17] D. Dai, M. H. Whangbo, H. J. Koo, X. Rocquefelte, S. Jobic, A. Villesuzanne, *Inorganic Chem.*, **44**, 2407 (2005).
- [18] J. L. Zarestky, D. Vaknin, B. C. Chakoumakos, T. Rojo, A. Goi, and G. E. Barberis, *J. Mag. Mag. Matt.* **234**, 401 (2001).
- [19] R. P. Santoro, R. E. Newnham, and S. Nomura, *J. Phys. Chem. Solids* **27**, 655 (1966); R. P. Santoro, D. J. Segal, R. E. Newnham, *J. Phys. Chem. Solids* **27**, 1192 (1966).
- [20] R. P. Santoro and R. E. Newnham, *Acta. Cryst.* **22**, 344 (1967).
- [21] D. Vaknin, J. L. Zarestky, J. E. Ostenson, B. C. Chakoumakos, A. Goñi, P. J. Pagliuso, T. Rojo, and G. E. Barberis, *Phys. Rev. B*, **60**, 1100 (1999).
- [22] D. Vaknin, J. L. Zarestky, L. L. Miller, J. -P. Rivera, and H. Schmid, *Phys. Rev. B*, **65**, 224414 (2002).
- [23] J. Li, V. O Garlea, J. L. Zarestky, and D. Vaknin, *Phys. Rev. B* **73**, 024410 (2006).
- [24] W. Tian, J. Li, J. W. Lynn, J. L. Zarestky, and D. Vaknin, *Phys. Rev. B* **78**, 184429 (2008).
- [25] T. B. S. Jensen, N. B. Christensen, M. Kenzelmann, H. M. Rønnow, C. Niedermayer, N. H. Andersen, K. Lefmann, J. Schefer, M. v. Zimmermann, J. Li, J. L. Zarestsky, and D. Vaknin, *Phys. Rev. B* **79**, 092412 (2009).
- [26] Y. Kharchenko, N. Kharchenko, M. Baran and R. Szymczak, *Low Temp. Phys.* **29**, 579 (2003).
- [27] D. Arčon, A. Zorko, P. Cevc, R. Dominiko, M. Bele, J. Jamnik, Z. Jaglicic, I. Golosocsky, *J. Phys. Chem. Solids*, **65**, 1773 (2004); D. Arčon, A. Zorko, R. Dominko, Z. Jaglicic, *J. Phys. Chem. Solids.*, **16**, 5531 (2004).
- [28] B. van Aken, J.-P. Rivera, H. Schmid, and M. Fiebig, *Nature* **449**, 702 (2007).
- [29] T. B. S. Jensen, N. B. Christensen, M. Kenzelmann, H. M. Rønnow, C. Niedermayer, N. H. Andersen, K. Lefmann, M. Jiménez-Ruiz, F. Demmel, J. Li, J. L. Zarestky, and D. Vaknin, *Phys. Rev. B* **79**, 092413 (2009).
- [30] V. I. Fomin, V. P. Genezdilov, V. S. Kurnosov, A. V. Peschanskii, A. V. Yeremenko, H. Schmid, J. -P. Rivera, and S. Gentil, *Low Temp. Phys.*, **28**, 203 (2002).
- [31] A. C. Larson, R. B. Von Dreele, and M. Lujan Jr., *Computer code GSAS, Generalized Structure Analysis System*, Neutron Scattering Center, Los Alamos National Laboratory, 1990.
- [32] V. A. Streltsov, E. L. Belokoneva, V. G. Tsirelson and N. K. Hansen, *Acta Crystal.*, **B49**, 147 (1993).
- [33] G. Rousse, J R. Carvajal, S. Patoux and C. Masquelier, *Chem. Mater.*, **15**, 4082 (2003).
- [34] M. F. Collins, *Magnetic Critical Scattering*, New York, Oxford University Press, 1989, p29.
- [35] D. Vaknin, J. L. Zarestky, J. -P. Rivera, and H. Schmid, *Phys. Rev. Lett.*, **92**, 207201/1 (2004).
- [36] H. Q. Ding and M. S. Makivić, *Phys. Rev. B*, **42**, 6827 (1990).
- [37] G. L. Squires, in *Introduction to the Theory of Thermal Neutron Scattering*, Cambridge University Press, New York, 1978, P156.
- [38] T. Nagamiya, *Solid State Physics* edited F. Seitz and D. Turnbull (Academic, New York, 1967), Vol. 29, p. 346.
- [39] J. H. Ranicar and P. R. Elliston, *Phys. Lett.* **25A**, 720 (1967).
- [40] P. R. Elliston, J. G. Creer, and G. J. Troup, *J. Phys. Chem. Solids* **30**, 1335 (1969).
- [41] O. Nagai, *Phys. Rev.* **180**, 557 (1969).
- [42] M. Bloch, *Phys. Rev. Lett.* **9**, 286 (1962), and *J. Appl. Phys.* **34**, 1151 (1963).